Catalytic pyrolysis and kinetic study of glass fibre-reinforced epoxy resin over CNTs, graphene and carbon black particles/ZSM-5 zeolite hybrid catalysts

Samy Yousef[1] · Justas Eimontas[2] · Nerijus Striūgas[2] · Marius Praspaliauskas[3] · Mohammed Ali Abdelnaby[4]

Abstract

The recovery of short fibre and epoxy resin from glass fibre-reinforced epoxy resin composites (GFRP) poses a major challenge to the waste recycling sector. These challenges grow when GFRP is mixed with other additives such as carbon nanotubes (CNTs), graphene (GA), and carbon black particles (CB). However, the complexity in terms of activation energy (E_a) can be decreased through involvement of ZSM-5 zeolite catalyst in the pyrolysis process to convert resin component into chemical and energy products. Within this context, this research aims to study the catalytic pyrolysis of GFRP mixed with three fillers with different structures and dimensions (nanofillers "CNTs, GA" and micro-filler "CB") over zeolite catalyst, where these fillers can be used alongside zeolite particles as hybrid catalysts during the thermal conversion process. The GFRP mixed with different filler panels were prepared in the laboratory using a vacuum-assisted resin transfer method, then they were ground to fine particles and mixed with 200 mass% of ZSM-5 catalyst to prepare them for thermochemical experiments using thermogravimetry (TGA) at 5–30 °C min^{-1}. The effect of various hybrids on the formulated pyrolysis vapours was studied using TG-FTIR and GC–Ms measurements. The kinetic E_a of each batch was studied using three linear isoconversional methods and two nonlinear isoconversional methods to investigate their effect on the decomposition mechanism. Besides, their thermochemical decomposition curves (TGA-DTG) were numerically simulated using DAEM and IPR models. The FTIR and GC analyses revealed that the hybrid catalyst had enhanced formation of aliphatic compounds and phenol compound in case of nanofillers up to 54% (CNTs) and 57% (GA), hence improving them by 17 and 54%, respectively. Meanwhile, the kinetic analysis showed that hybrid catalysts can contribute to a significant reduction in E_a up to 158 kJ mol^{-1} (CNTs), 127 kJ mol^{-1} (GA), and 124 kJ mol^{-1} (CB), which means that the decomposition of GFRP, becomes easier and requires less energy. Also, the simulated and experimental results showed big consistency in terms of smaller reaction complexity and higher generation of volatile compounds with increasing heating rates and addition of hybrid catalysts.

Keywords Glass fibre-reinforced epoxy resin · Carbon nanotubes · Graphene · ZSM-5 zeolite catalyst · TG/FTIR-GC/MS analysis · Catalytic pyrolysis kinetic behaviour

✉ Samy Yousef
ahmed.saed@ktu.lt

1 Department of Production Engineering, Faculty of Mechanical Engineering and Design, Kaunas University of Technology, 51424 Kaunas, Lithuania

2 Laboratory of Combustion Processes, Lithuanian Energy Institute, Breslaujos 3, 44403 Kaunas, Lithuania

3 Laboratory of Heat Equipment Research and Testing, Lithuanian Energy Institute, Breslaujos 3, 44403 Kaunas, Lithuania

4 Mechatronics Systems Engineering Department, October University for Modern Sciences and Arts-MSA, Giza, Egypt

Introduction

For a long time, the waste of glass fibre-reinforced thermosetting resin (GFRP) composites has been causing big inconveniences to recycling industry and those interested in environmental matters [1, 2]. Currently, these challenges have increased greatly due to waste use in many advanced applications such as wind turbine blades, aerospace structure, and electronic industries because of its high mechanical properties, low density, low electrical conductivity, long service life, etc. [3, 4]. Besides, due to its simplicity in producing required shapes, cheap, high chemical, thermal, and fire resistance, the increased demand for it has been noticed

in traditional applications such as defense, automobiles, ships, concrete industry, aircraft structure, etc. [5–8], hence increasing the consumption rate of fabric by 6% annually [9]. Based on that, tremendous amounts of GFRP waste composed of epoxy resin (40 mass%) and several layers of glass fabrics joined together by complex covalent intermolecular bonds are generated, making it difficult to treat them mechanically, thus making landfill or incineration treatment the most ordinary practices [10–12]. However, these practices have several limitations with regard to their economic performance and environmental pollution. Even mechanical practice, including milling, crushing, and shredding process used as a pre-treatment to reduce size and to convert GFRP waste into short fibres, manifested low performance compared with neat fibre as a result of its contamination with epoxy resin, which affects bonding in the matrix like cementitious, wood, polymer matrix composites [7, 13]. Even treatment of the recovered fibre using chemical treatment for purification process with organic solvents or supercritical fluids consumes too many chemicals, resulting in numerous chemical waste and toxic emissions [14–16].

Therefore, the researchers' attention was turned towards thermal treatment like pyrolysis process used to decompose the epoxy particles into vapours and gases above 450 °C with high additional valuable compounds, such as benzene and phenol compounds, while, glass fibre particles remain in the solid residue [17, 18]. This process is classified as an emerging and clean technology with less emissions and the experiments can be carried out on a few mg using thermogravimetry (TGA) to determine the thermal decomposition regions of GFRP [19]. Meanwhile, the compositions of the pyrolysis compounds produced from the decomposition experiments can be indicated using TGA combined with Fourier transform infrared (TG-FTIR) spectroscopy and gas chromatography–mass spectrometry (GC/MS) under various heating parameters. Based on that, the activation energies which are used to define the complexity of the reaction as a function on conversion zones were calculated using different kinetics isoconversional approaches [20]. The results showed that the fabric fraction tends to increase the complexity of the reaction, thus consuming more energy to achieve complete decomposition during the conversion process. Moreover, thermal decomposition of GFRP was also investigated using a pilot scale pyrolysis reactor to get the real products and to calculate their yield [21]. In addition, the effect of involvement of different types of filler materials (carbon nanotubes "CNTs", graphene "GA", and carbon black"CB") on the pyrolysis performance of GFRP and its kinetic behaviour and other measurements (e.g. TAG, FTIR, GC/MS) was studied again [22, 23]. The results showed that these additives have a significant effect on the formulated pyrolysis products, especially phenol compound (main organic element in epoxy resin), where these fillers

act as self-catalysts helping to increase the yield of the recovered phenol up to 46% at 10 °C min⁻¹ (CNTs), 37% at 15 °C min⁻¹ (GA), and 67% at 30 °C min⁻¹ (CB). Whereas, the maximum abundance of phenol compound was achieved in neat GFRP feedstock at 10 °C min⁻¹ (43%) [19].

In order to decrease the complexity of reaction and to improve quality of the products and to increase the calorific value and yield, GFRP was exposed to catalytic pyrolysis treatment using different types of catalysts such as HZSM-5 (20–500 mass%) and ZSM-5 (catalyst to feedstock ratio (w/w); 0.5–5) [24, 25]. These catalysts help to generate a large amount of mono-aromatic hydrocarbons, the number of which is increased in case of ZSM-5 catalyst, especially at ZSM-5/GFRP = 2 with phenol abundance estimated at 66% at 5 °C min⁻¹ [25]. As shown, most studies were focused on the catalytic pyrolysis of GFRP (as received) only, whereas, the catalytic pyrolysis of GFRP mixed with other additives (e.g. CNTs, GA, CB) is still unknown, however, these properties and their kinetic should be known for potential upscaling at industrial scale, especially as these additives act as self-catalysts and hybrid catalysts (with the main used catalyst) and are able to contribute to reduction of complexity of the reaction and improvement of heating values. Within this frame, this work aims to study the catalytic pyrolysis of GFRP mixed with various types of fillers (CNTs, GA, and CB) over ZSM-5 zeolite catalyst (ZSM-5/feedstock ratio = 2) using TG-FTIR and GC–MS analysis. The experiments were performed using nano-filler materials (CNTs and GA) and another filler in micro-scale size (CB) to study the effect of fillers structure, geometry, and dimensions on their thermal decomposition properties. Also, the kinetic modelling of GFRP over hybrid catalysts and their decomposed thermochemical curves was applied, as these models are needed to bridge the gap between laboratory scale and industrial practices. Finally, the influence of the hybrid catalysts (CNTs/ZSM-5, GA/ZSM-5, and CB/ZSM-5), heating rates and testing parameters on reaction mechanisms were analysed.

Experimental

Feedstock preparation and catalyst characterization

The GFRP reinforced by CNTs, GA, and CB panels used in the current work were fabricated in the laboratory using vacuum-assisted resin transfer method. The fillers used in the preparation had 25 nm (CNTs), 18 nm (GA), and 10–15 μm (CB), respectively [22, 26, 27]. The composite panels with thickness of 1 mm were composed of 60 mass% of 4 layers of glass fabric Panda™ (Weave: Twill 2/2 type and mass: 163 g m⁻²), 45 mass% of epoxy resin, 15 mass% of hardener (EPIKOTE Resin MGS® RIMR 135 and EPIKURE Curing

Agent MGS® RIMH 1366), and 0.04 mass% of CNTs or GA or 0.75 mass% of CB. The percentages of filler materials were selected based on the optimum conditions used to achieve higher mechanical performance of composite panels and reported in the literature [5, 28, 29]. The feedstock was used in the experiments by grinding the fabricated panels into small particles, then saving them to obtain fine particles (300 μm) with uniform distribution. Approximate parameters were measured in our recent study, which were estimated at 40% (Volatile Matter), 2% (Fixed Carbon), and 6% (Ash) [22, 23]. The used catalysts (ZSM-5 zeolite) were purchased from ACS MATERIAL advanced chemical supplier, Germany, and had the following characteristics: SiO2/Al2O3 molar ratio was 38, pore volume ≥ 0.25 mL g^{-1}, dimensions of granules were 2 mm in diameter and 2–10 mm in length, and pore size of ~5 Å [30, 31]. Finally, each batch was given an abbreviation based on type of fillers, ZSM-5 zeolite catalyst (ZS), and GFRP (GP), in particular, ZS/CNTs-GP (CNTs, ZSM-5, and GFRP), ZS/GA-GP (GA, ZSM-5, and GFRP), and ZS/CB-GP (CB, catalyst, and GFRP).

Thermogravimetric experiments

The catalytic pyrolysis experiments of GFRP over hybrid catalysts were carried out using the thermogravimetric analyser (TGA; model: STA449 F3; NETZSCH, Selb, Germany) in nitrogen ambient with flow rate of 60 mL min^{-1} and sample mass of 10 mg and the weight of added ZSM-5 catalyst was 20 mg. The measurements were conducted at varying heating conditions (5, 10, 15, 20, 25, 30 °C min^{-1}) at a room temperature of 40 °C and at maximum temperature of 900 °C, which was also needed for kinetic analysis. The mass loss was recorded using Pyrys software followed by plotting TGA curves, then obtaining DTG information through derivation of TGA results. In order to increase the accuracy of the analysis and pyrolysis kinetic results, all TGA measurements were performed three times and an average value was taken. Based on the calculated DTG data, the devolatilization index (D_i) and the heat-resistance index (THRI) were determined using Eqs. (1, 2) [32, 33]. Definitions of all parameters used in the present work are listed in Table S1 in the Supplementary Materials section.

$$D_i = \frac{R_{max}}{(T_i) \times (T_m) \times (\Delta T)} \tag{1}$$

$$THRI = 0.49 \times [T_5 + 0.6 \times (T_{30} - T_5)] \tag{2}$$

Chemical analysis of the obtained volatile compounds

The generated pyrolysis vapours and gases from catalytic pyrolysis of GFRP mixed with fillers at the maximum degradation region were analysed using (Vertex70 spectrometer) FTIR combined with the thermogravimetric analyser. Also, these products were collected using automatic Auto-injector™, and then analysed again using gas chromatography–mass spectrometry (GC/MS, Thermo Scientific ISQ™ single quadrupole) to determine their main composition. The GC/MS measurements were conducted using column setting with the following characteristics: Argon ≥ 99.999%, 20 psi, and 95 °C injector temperature [34, 35].

Catalytic pyrolysis kinetics of GFRP samples

To describe the mechanism of the catalytic pyrolysis kinetics of GFRP samples with additives, a kinetic analysis was used to determine the complexity for all samples. The complexity of the whole conversion process was determined using Kissinger model, as formulated in Eq. [3]. Also, according to ICTAC Kinetics Committee, the complexity can be determined by defining the relationship between activation energy (E_a) and conversion rate (y) using linear isoconversional model-free methods. These methods have several models, from which Kissinger–Akahira–Sunose (KAS), Flynn–Wall–Ozawa (FWO), and Friedman models were selected and used in the present research using Eqs. (4–6). However, linear models are very sensitive for noise data, thus affecting accuracy of the calculated E_a. Therefore, Vyazovkin and Cai nonlinear methods were used to calculate E_a using numerical integration algorithms. The basic formulas are shown in Eqs. (7, 8) and all equations are listed in Table 1.

Reconstruction of TGA and DTG curves using DAEM and IPR models

The thermal decomposition of TGA-DTG curves of GFRP for each lower and higher heating rates (5 and 30 °C min^{-1}) was reconstructed using the kinetic models of distributed activation energy (DAEM) and independent parallel reactions (IPR) based on activation energy ($E1$ and $E2$) and pre-exponential factor ($A1$ and $A2$), which can be calculated using Eqs. (9, 10) [38]. The experimental curves overlapped with their, respectively, reconstructed TGA and DTG curves and both curves were compared mathematically curves using deviation (Dev.%) formula, as described in Eq. (11) [39].

$$\ln\left(\frac{\beta}{T^2}\right) = \ln\left(\frac{AR}{E_a}\right) + 0.6075 - \frac{E_a}{RT} \tag{9}$$

Table 1 Formulas of linear and nonlinear isoconversional models [36, 37]

Eq. No	Method	Expressions	Plots	Slope value
(3)	Kissinger	$\ln\left(\frac{\beta}{T_m^2}\right) = \ln\left(\frac{AR}{E_a}\right) - \frac{E_a}{RT}$	$\ln\left(\beta/T_m^2\right)$ versus $1/T$	$-E_a/R$
(4)	Kissinger–Akahira–Sunose	$\ln\left(\frac{\beta}{T^2}\right) = \ln\left(\frac{AR}{Eag(y)}\right) - \frac{-Ea}{RT}$	$\ln(\beta/T^2)$ versus $1/T$	$-E_a/R$
(5)	Flynn–Wall–Ozawa	$\ln\beta = \left(\frac{\ln AEa}{Rgy}\right) - 5.335 - \frac{1.0516Ea}{RT}$	$\ln\beta$ versus $1/T$	$-1.0516E_a/R$
(6)	Friedman	$\ln\left(\frac{\beta dy}{dT}\right) = \ln(Af(y))\left(\frac{-Ea}{RT}\right)$	$\ln(dy/dt)$ versus $1/T$	$-E_a/R$
(7)	Vyazovkin	$(\alpha) = \int_0^\alpha \frac{dy}{f(y)} = A\int_0^t \exp(-E/RT)dt$		$-E_a/R$
(8)	Cai	$\ln\left\{\frac{i}{T_{y,i}^2\left[h(x_{y,i}) - \frac{x_{y,i}^2 e^{x_{y,i}}}{x_{y-\Delta y,i}^2 e^{x_{y-\Delta y,i}}}h(x_{y-\Delta y,i})\right]}\right\} = \ln\left\{\frac{A_{y-y/2}R}{E_{y-y/2}\,g(y,y-y)}\right\} - \frac{E_{y-y/2}}{RT_{y,i}}$		$-E_a/R$

$$\frac{dm^{calc}}{dt} = -(m_0 - m)\sum_{i=1}^{3} C_i\frac{dX_i}{dt} \qquad (10)$$

$$\text{Dev.}(\%) = \frac{100\sqrt{\text{F.O.}_{DTG}(Z-N)}}{\max(|dm/dt|)} \qquad (11)$$

Results and discussion

Thermal behaviour of GFRP samples

Figure 1A–F shows the TGA and DTG profiles obtained for the catalytic pyrolysis of GFRP samples with different filler materials at under heating rates of 5, 10, 15, 20, 25, and 30 °C min^{-1}. TGA profiles (Fig. 1A–C) showed three different decomposition regions. The first mass-loss region up to 140 °C temperature is attributed to the evaporation of moisture in the feedstock and catalyst with a very small mass < 1 mass%. The second and third decomposition regions of mass loss at temperatures between 320 (3 mass%) and 460 °C (12 mass%) were determined by evaporation of chemical residues remaining from the production process in the second region followed by full degradation of all components of an epoxy resin fraction, including bromine element [40, 41]. Finally, the undecomposed fraction remaining as a solid residue fraction was composed of short fibreglass (which needs a higher temperature to decompose), carbon black, and the used catalyst. As shown, the total mass loss in all samples was estimated at 16 mass% due to thermal degradation of epoxy resin fraction only; however, these results conflict with the original mass of epoxy in the feedstock, which was estimated at 40%, as listed before. This conflict resulted from considering the mass of the used catalyst during plotting of

the decomposition profiles, as it has higher thermal stability and cannot decompose at such a low level. Therefore, the catalyst mass was removed from all calculations to obtain the accurate curves and the total mass loss was estimated at 50%, what means that involvement of the catalyst in the reaction did not affect significantly the whole mass loss and the main effect in the formulated compounds, as shown in the following sections [30]. On the other side, DTG profiles (Fig. 1D–F) showed that the maximum decomposition temperatures of the tested samples lie in the ranges of 420–540 °C. Also, the intensity of these peaks increased gradually as heating conditions increased due to the fact that higher heating rates led to bigger heat flux, thus facilitating the transfer of heat between the outer surface of the pyrolysed particles (suppose direct to heating source) and their inner molecules, thus speeding up the decomposition process [42]. Based on the TGA-DTG profiles, all catalytic pyrolysis characteristics of fillers/GFRP, including Di and THRI, were determined and all characteristics are summarized in Table 2.

It seems that the Di value of all samples increases with the increase of the heating rate, which facilitates the volatilization process and helps to enhance the release of volatiles since the devolatilization reaction is classified as an endothermic process, while the formation of solid residue fraction (char and fibres) is an exothermic process. Also, the higher heating rate led to reduce the residence time of the tested sample at low temperature what led to an inhibiting condensation reaction and enhancing the devolatilization reaction. It can be seen that the Di value of the samples decomposed over catalyst is larger than that of the sample decomposed without catalyst at the same heating rate [43]. On the other hand, the THRI values of ZSM-5/fillers/GFRP samples were observed to fall in the ranges of 324–331 °C.
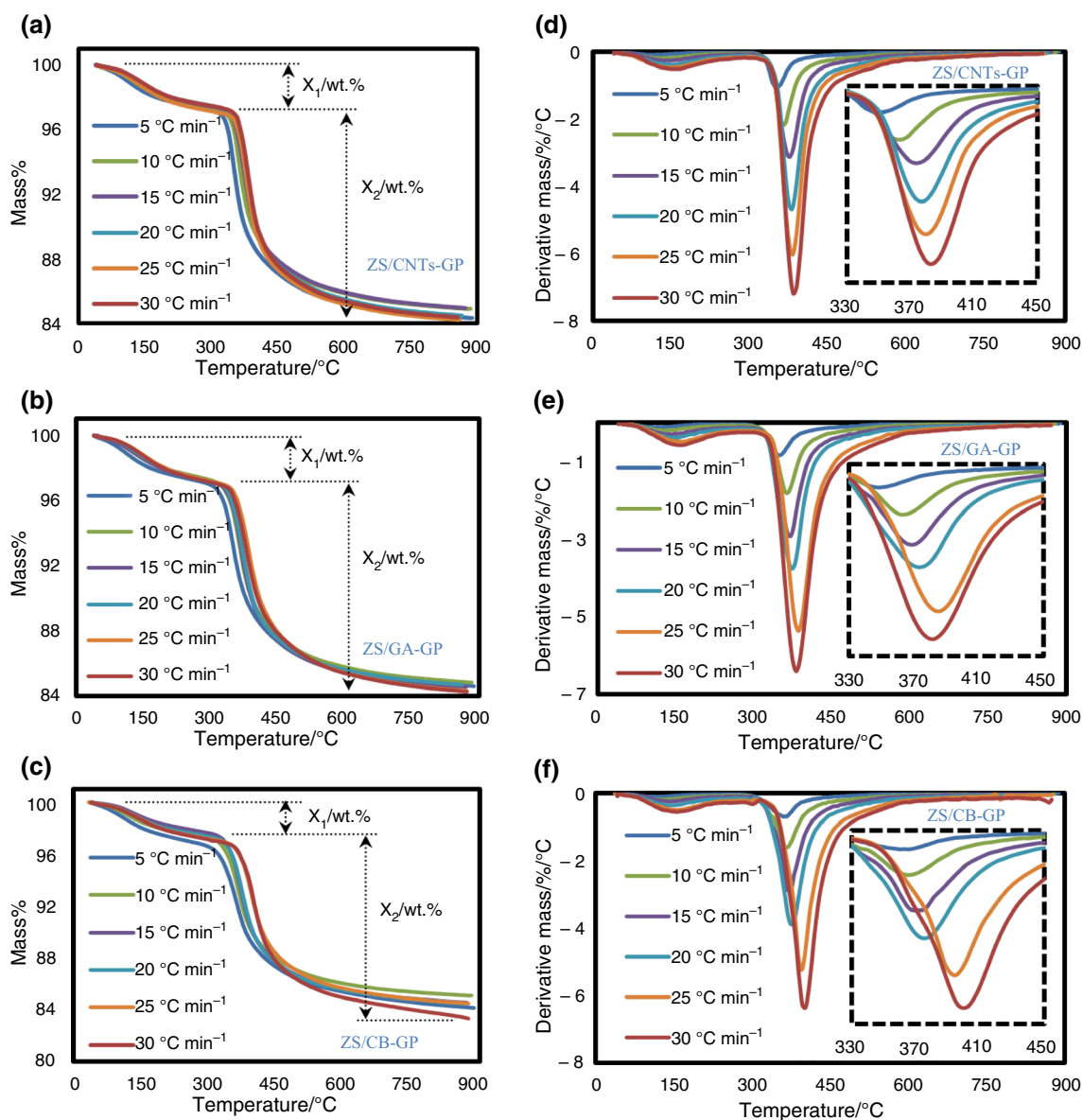
Fig. 1 **A–C** TGA analysis and **D–F** DTG profiles of ZSM-5/fillers/GFRP samples

When compared with the THRI value of the fibre/epoxy sample (without catalyst: 166–178 °C [19]), the THRI values of the ZSM-5/filler/GFRP samples increased with the addition of CNT, GA and BC fillers due to the chemical modification of epoxy resin and its high thermal stability [44].

FTIR analysis of the formulated compounds

The functional groups existing in the vapour pyrolysis and gaseous compounds were identified using the TG-FTIR system. Figure 2 shows the 2-3D FTIR spectra of pyrolytic compounds of ZSM-5/fillers/GFRP samples produced in the maximum degradation region and under various heating rates. The tested samples have similar chemical bonds

and all the corresponding peaks are defined in Table 3. In all batches, O–H stretching (3646 cm^{-1}), CO_2 group (2956 cm^{-1}), and aromatic benzene group (1186 cm^{-1}) represent the main broad bands [19]. The uptake of these functional groups also increases significantly with increasing heating conditions and heat flux; besides, the epoxy resin molecules are broken into smaller molecules and converted into volatile and chemical compounds faster [45]. These features were observed in the FTIR spectra of the compounds obtained from pyrolysis of GFRP, but the intensity of CO2 band at 2352 cm^{-1} was a little bit smaller. Meanwhile, in case of ZSM-5/GFRP sample, this group was a little bit sharper [25]. In the same direction, 3D FTIR spectra showed that the peaks become

Table 2 Catalytic pyrolysis characteristics of ZSM-5/fillers/GFRP samples under various heating conditions

Pyrolysis parameters	ZS/CNTs-GP, Heating rate/°C min^{-1}					
	5	10	15	20	25	30
Ti/°C	306	324	329	330	324	330
Tm/°C	352	363	375	378	380	381
Tf/°C	554	541	569	565	579	601
Rmax/% min^{-1}	1.08	2.17	3.11	4.69	6.03	7.19
Di/% min^{-1} °C^{-3}	2.9E-07	4.7E-07	5.5E-07	9.9E-07	1.2E-06	1.2E-06
ΔT	34	39	46	38	40	46
T5	344	358	365	367	368.9	369
T30	888	884	873	865	860	856
THRI	328	330	328	326	325	324
	ZS/GA-GP, Heating rate (°C min^{-1})					
Ti/°C	298	302	303	321	332	311
Tm/°C	348	366	578	374	385	607
Tf/°C	583	589	370	575	577	602
Rmax/% min^{-1}	0.85	1.81	2.93	3.76	5.38	6.4
Di/% min^{-1} °C^{-3}	1.8E-07	3.7E-07	3.6E-07	5.9E-07	7.4E-07	5.7E-07
ΔT	45	44	46	53	57	60
T5	362	366	358	355	351	337
T30	871	872	862	871	883	888
THRI	327	328	324	326	328	327
	ZS/CB-GP, Heating rate/°C min^{-1}					
Ti/°C	290	306	309	319	318	331
Tm/°C	365	365	371	378	394	402
Tf/°C	564	570	583	589	593	604
Rmax (% min^{-1})	0.7	1.58	2.9	3.87	5.25	6.37
Di/% min^{-1} °C^{-3}	1.1E-07	2.9E-07	5.0E-07	5.9E-07	9.3E-07	8.1E-07
ΔT	58	49	51	54	45	59
T5	336	350	361	362	377	378
T30	888	883	871	864	875	875
THRI	327	328	327	325	331	331

smoother as heat was growing, and less disturbance peaks were reached. Therefore, it is highly recommended to use stronger heating during the thermochemical treatment of GFRP mixed with fillers to decompose all of epoxy molecules during shorter reaction time.

GC–MS analysis of the formulated volatile product

Figure 3 illustrates the GC/MS spectra of volatile products at the maximum peak in the specified heating ranges (5–30 °C min^{-1}) for all ZSM-5/fillers/GFRP samples, while the normalized peak areas of the formulated organic compounds are shown in Table [S2–S4]. As shown, the type of filler and heating conditions have a significant effect on the formulated organic compounds in the volatile products produced form catalytic pyrolysis of GFRP. However, phenol compound was the main element in all decomposed samples, even with changing heating rates, yet the abundance was different as shown in Fig. 4.

It was estimated as 54% at 5 °C min^{-1} (ZS/CNTs-GP), 57% at 10 °C min^{-1} (ZS/GA-GP), and 59% at 25 °C min^{-1} (ZS/CB-GP). The increase was noticeable, when compared with the virgin GFRP (43% at 25 °C min^{-1}) and the same composite batches without catalyst [19, 23]. Meanwhile, the results were not much smaller when compared with ZSM-5/GFRP and CB/GFRP [22, 25], where the abundance of phenol was increased by adding ZSM-5 by 53% (GFRP), 17% (CNTs/GFRP), 54% (GA/GFRP). In case of CB/GFRP, it decreased by 12%, as shown in Fig. 5. As shown, the maximum phenol yield was obtained from ZS/CNTs-GP and ZS/GA-GP at low heating rates, while in the case of ZS/CB-GP it was obtained at a higher heating rate. This is due to the high thermal conductivity of CNTs and GA nanomaterials that accelerate the heat transfer between the outer surface of the pyrolysed particles faster and accelerate the decomposition reaction [46]. On the contrary, the pristine GFRP sample has a poor thermal conductivity which needs higher heating conditions for better heat exchange and complete

Fig. 2 2-3DFTIR analysis of vapour pyrolysis compounds generated from ZSM-5/fillers/GFRP samples
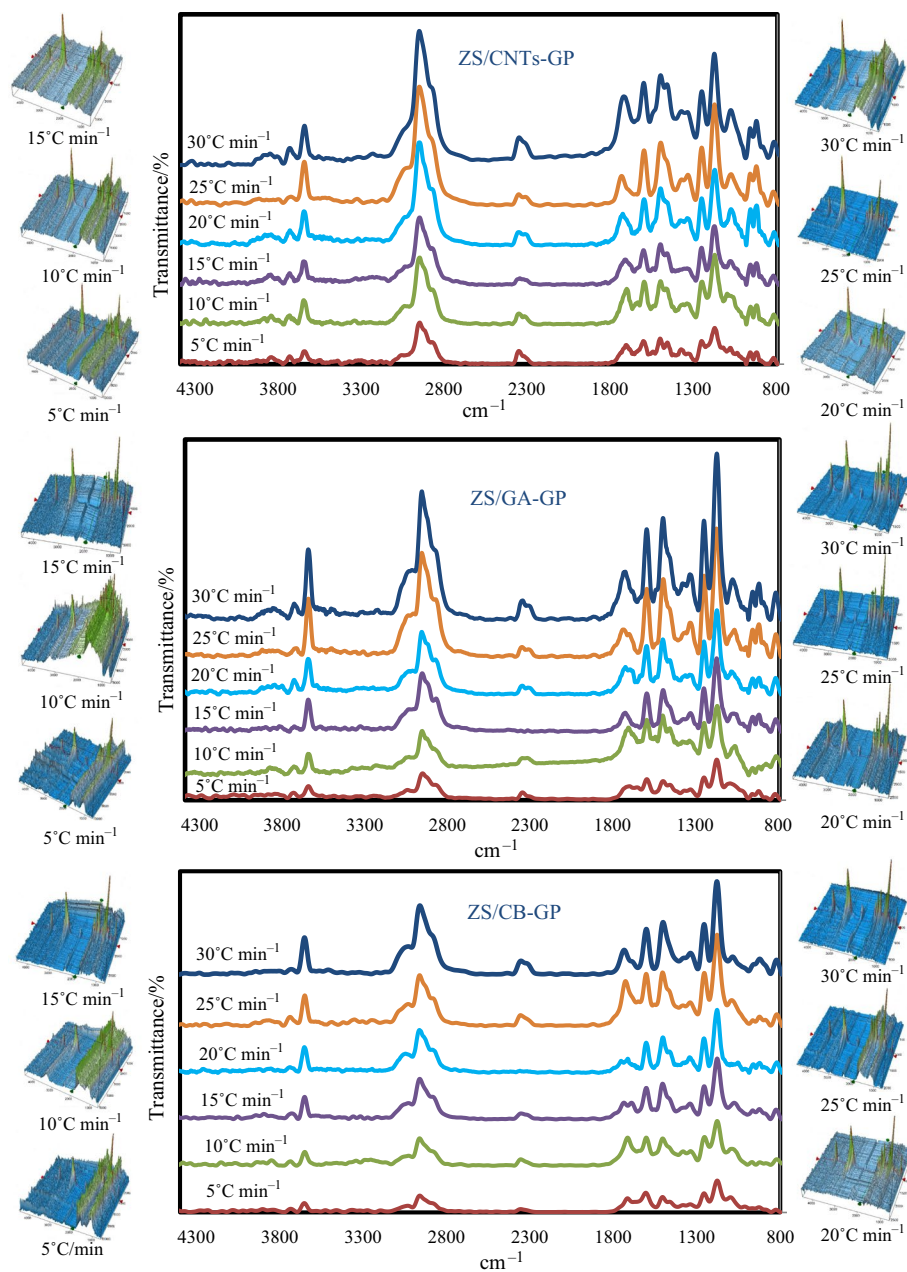
Table 3 Definitions of the functional groups of the formulated vapour pyrolysis compounds

Wavelength/cm^{-1}	Functional group definition
3646	O–H stretching
2956	CO2 group
2360	band of CO2
1725	carbon-yl (C=O)
1300–1494	N–O group
1186	Aromatic benzene group

degradation [47]. Besides, CNT and GA fillers a higher surface to volume ratio that helps in increasing the contact surface between the fillers and the volatile compounds generated. In addition, the relatively large size of the CB (upto 15 µm) can clog the pores of the catalyst used in the upgrading process [25]. This means that this kind of fillers has a significant effect on catalytic pyrolysis of GFRP, yield of the recovered phenol and the composition of the other formulated compounds, in addition to the effect of catalyst which helps to enhance the volatile products [48]. Besides, the effect of heating conditions plays an important role in the heat flux produced during the reaction [49]. Also, some boron-based compounds were observed in the GC–MS
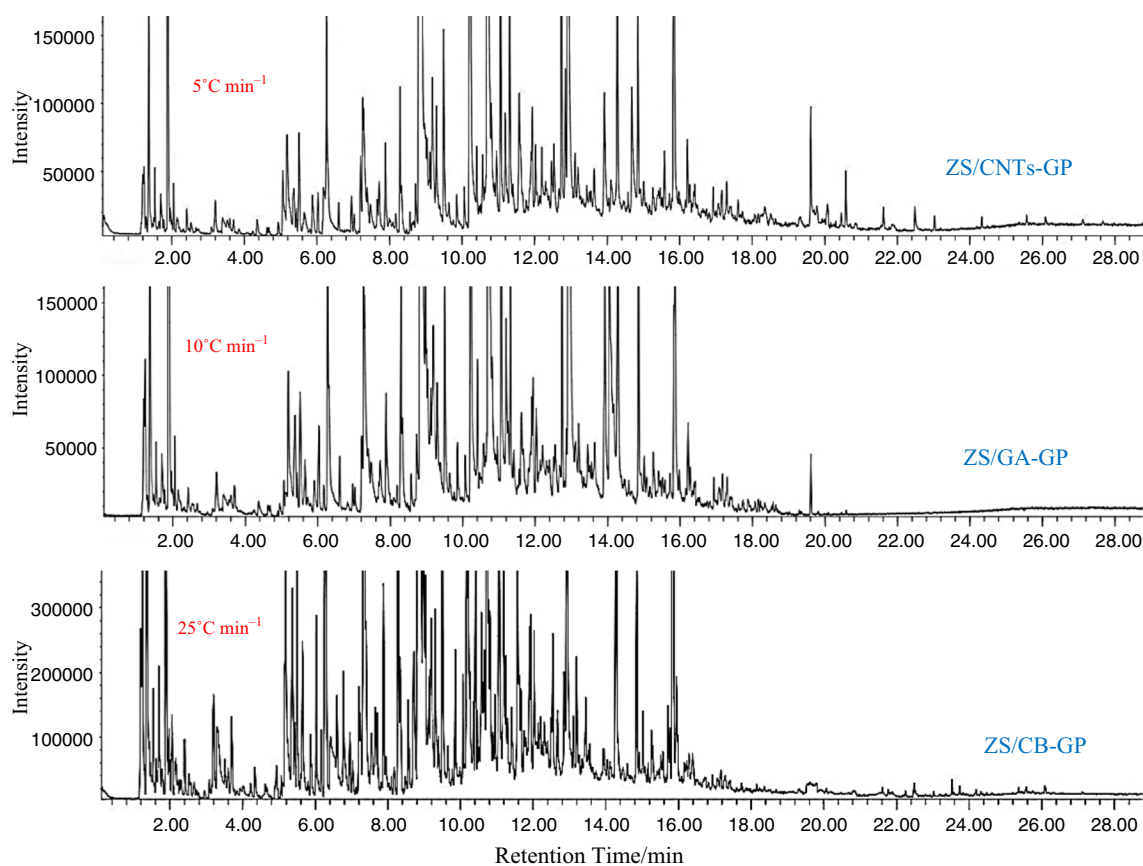
Fig. 3 GC–MS analysis of the decomposed ZSM-5/fillers/GFRP samples

Fig. 4 Abundance of the phenol compound recovered from ZSM-5/fillers/GFRP samples at different heating rates (5–30 °C min^{-1})
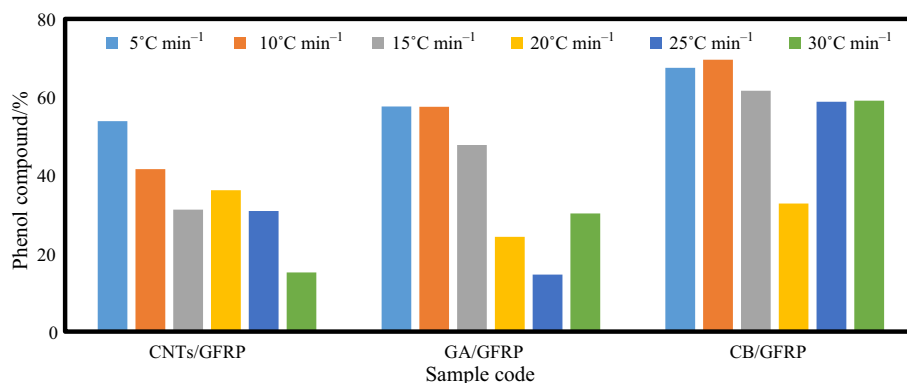

results due to fact that boron can be used as curing agents to increase the thermal stability and flammability of epoxy resins during its production process [50, 51]. Therefore, the catalytic pyrolysis process over ZSM-5 is a very recommended technology to treat GFRP mixed with nanofillers (like CNTs and GA) to recover phenol from them, while its performance is not good with regard to such micro-particles as CB. Finally, the recovered phenol and other compounds can be used in several advanced applications, including chemical and renewable energy fields [52–54].

Catalytic pyrolysis mechanism of fillers/GFRP

The feedstock was composed of short fibreglass, epoxy resin, and filler materials (CNTs, GA, and CB). The thermochemical process can help to decompose organic fraction only (epoxy resin), while fibreglass remains as a residue, and the filler material acts as a self-catalyst. The decomposition mechanism of the samples and their complexity were studied in this part based on TGA measurements supported by GC/MS results. Since the highest amount of phenol
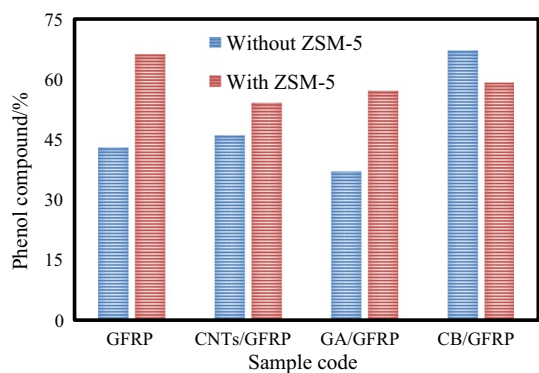
Fig. 5 Abundance of the phenol compound recovered from GFRP samples in presence and without ZSM-5 catalyst [19, 22, 23, 25]

compound was recovered from ZS/CNTs-GP, ZS/GA-GP, and ZS/CB-GP at 5 °C min^{-1} (based on GC/MS measurements), the proposed mechanism was built and discussed based on these samples and conditions, then compared to the GFRP mechanism published by our team earlier. Figure 6 displays the proposed mechanism of the selected samples under the applied heating conditions and in presence of a catalyst, according to the TGA results. Regardless of the type of fillers, the mechanism starts with evaporation of moisture presented in catalyst and feedstock together up to 155 °C, then followed by evaporation of chemical residues from various production processes up to 320 °C. Besides, the glass fibres were dismantled from epoxy resin debris by breaking the friction and chemical bonds between them [55]. As shown, filler types and catalyst adding did not play

any role in these regions since the profiles in these areas are fully matched. After that, the applied heating penetrated through epoxy resin debris and broke down their internal van der Waals' bonds and their chain scission into smaller molecules followed by recombination of the reactions and formulation of its basic compound (phenol) up to 460 °C [56]. The amplitude of phenol compound was changed by type of filler materials and also the heating rate applied, as shown in GC/MS analysis, where smaller molecules had very low crystallinity allowing hybrid catalysts (CNTs, GA, CB/ ZSM-5) to react with them in highly effective catalytic reactions through dihydroxylation and cracking of phenol and bisphenol, then debromination of brominated elements from them followed by decomposition into aromatic hydrocarbons with significant selectivity towards monophenol compound [16, 41, 57].

This is due to the fact that ZSM-5 catalyst has a large porosity allowing brominated elements to diffuse smoothly in their structure and to perform the debromination process with high efficiency. Besides, its stronger acidity and selectivity of aromatic compounds led to cumulatively large amount of phenol compound compared with decomposed samples without catalyst [18, 58]. Also, in these organic fractions can decompose only, while CNTs, GA, and CB cannot decompose at such low temperatures, where these fillers can decompose above 650 °C and convert into CO2 [59–61]. However, these undecomposed fillers precipitated on the surface of ZSM-5 particles and formed hybrid catalysts (CNTs, GA, CB/ ZSM-5) leading to acceleration of the breakage rate generating more gaseous and hydrocarbons compounds [36]. This bonding depended on the contact
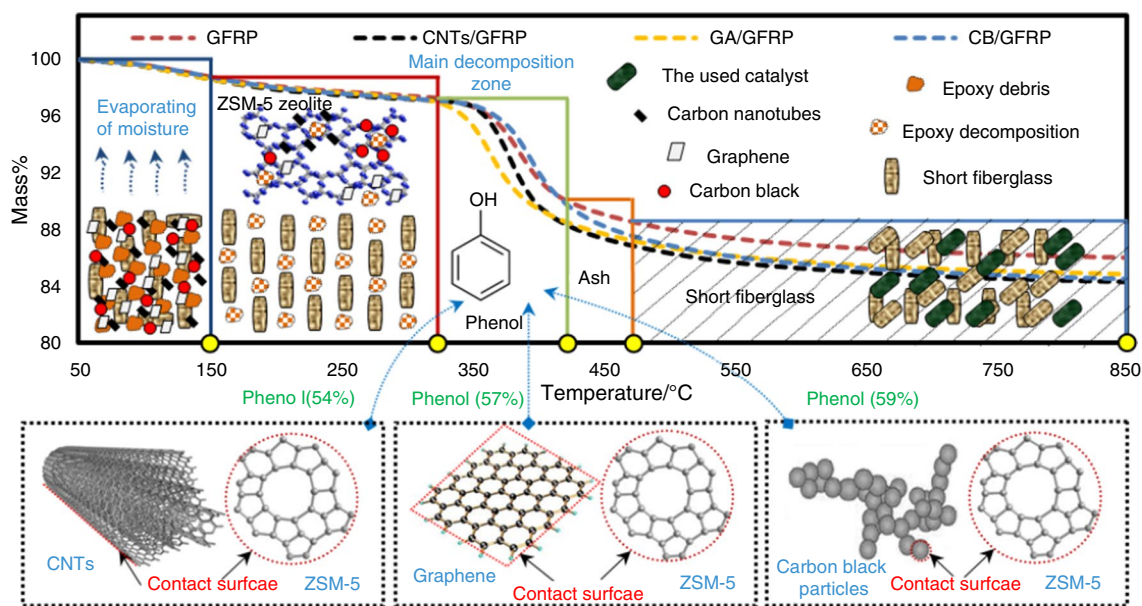
Fig. 6 Mechanism of ZSM-5/fillers/GFRP pyrolysis

between filler and catalyst, where CNTs and GA had a ratio and surface to volume ratio higher than CB particles leading to higher contact with ZSM-5, thus acting as a single catalyst with double selectivity performance [62, 63]. While CB has a lower surface to volume ratio (compared to CNTs and GA) and larger particle size (up to 15 μm) it can clog the pores of the ZSM-5 catalyst what is the effect on the performance of the phenol extraction process [22, 25]. Finally, the non-composed components, short fibreglass, and the used catalyst remained in the form of ash and solid residue in the last regions, which can be used as filler material for concrete or in composite applications in general [64, 65].

Kinetic study results

Activation energy for the entire thermochemical process

Kissinger model using Eq. (3) was used to evaluate the complexity of the entire thermochemical process in terms of total activation energy (E_{tot}). The E_{tot} value for each sample was determined by plotting the linear relationship between $\ln\left(\beta/T_3^2\right)$ and $1/T$, then determining the slop of these curves, which is defined as $-E_a/R$ and $R = 8.31\ JK^{-1}\ mol^{-1}$ and the fitted Kissinger curves are shown in Fig. 7. The calculation showed that ZS/CNTs-GP, ZS/GA-GP, and ZS/CB-GP samples had E_{tot} estimated at 157 kJ mol^{-1}, 147 kJ mol^{-1}, and 105 kJ mol^{-1}, respectively. It seems that all samples with nanofillers had almost the same E_{tot}, while the difference from the micro-filler sample was big. Also, compared to GFRP (126 kJ mol^{-1}), ZSM/GFRP (161 kJ mol^{-1}), CB/GFRP (182 kJ mol^{-1}), CNTs/GFRP (155 kJ mol^{-1}), GA/GFRP (176 kJ mol^{-1}) samples [19, 22, 23, 25], ZSM/fillers/GFRP samples had lower Etot what indicates that pyrolytic decomposition process became easier than the case of without a catalyst. Whereas the variation in the fitted data due to the simplicity of the Kissinger model which was built on the basis of a single reaction approach without too much assumptions [66]".

Activation energy for each conversion region

The complexity of each conversion (y) for the entire thermochemical process was estimated in term of activation energy (E_a) using three linear isoconversional models (Kissinger–Akahira–Sunose (KAS), Flynn–Wall–Ozawa (FWO), and Friedman) and two nonlinear isoconversional models (Vyazovkin and Cai).

Linear isoconversional models By using these models, E_a was determined using the curve fitting method for each model, then E_a was calculated from the slope term of each fitting curve. Figure 8 shows the fitted KAS, FWO, and Friedman models in the conversion ranges of 10–90% using Eqs. (4–6). KAS and FWO fitted curves were composed of parallel straight lines in the ranges 20–90%, while at the lowest conversion zone ($y = 10\%$), they showed random distribution. Whereas, Friedman curve showed overlapping straight lines with several disturbances in the main degradation regions with a little random distribution also at $y = 10\%$. Due to of parallel reactions resulting from changes in the composition of feedstock and produced from catalyst and filler materials leading to significant changes in the chain size of organic fraction present in the feedstock [21, 67]. Friedman approach is very sensitivity to noise data obtained during the measurements, what effected the accuracy of results of E_a. Based on that, KAS and FWO linear isoconversional are suitable models to investigate the reaction mechanism of ZSM/fillers-GP samples above 10% until the end of reaction. All values of the calculated E_a obtained from each model and its coefficient of determination (R2) as a function of conversion rate are shown in Fig. 9 and Table S5. It was noticed that the activation energy as a function of conversion increases and decreases due to the fact that the feedstock contains a larger number of pseudo-components and pseudo-subcomponents (e.g. fibres, epoxy, hardener, fillers, other additives, etc.) which decomposed individually during the conversion process. Each element of these components
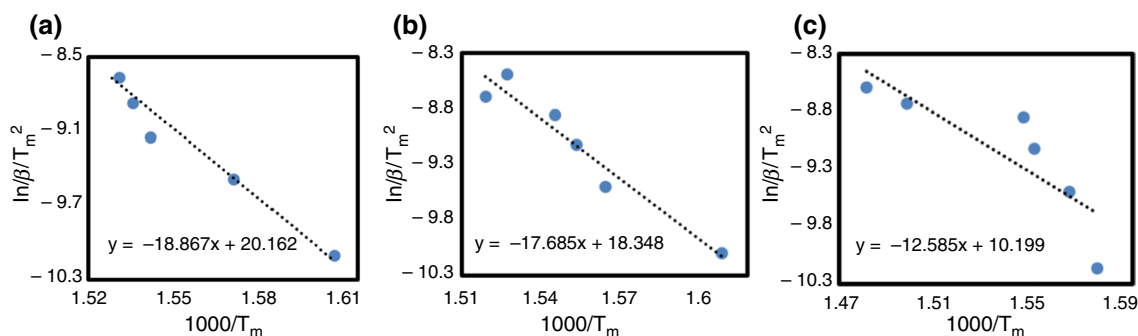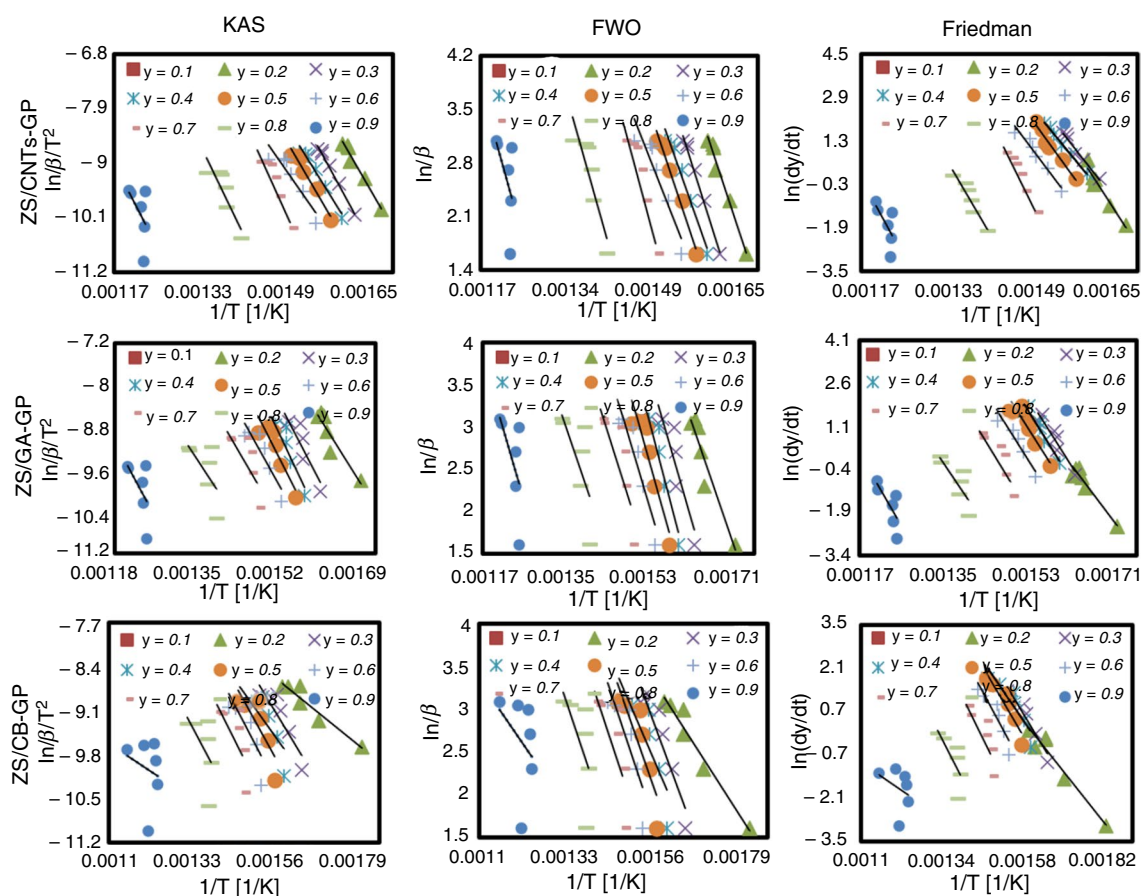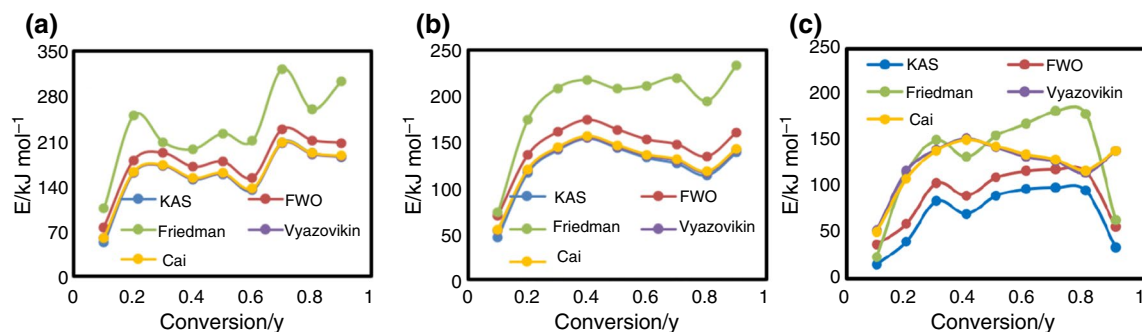

Fig. 7 Plots of Kissinger relationships of **A** ZS/CNTs-GP, **B** ZS/GA-GP, and **B** ZS/CB-GP samples

**Fig. 8** Plots of linear isoconversional curves of ZSM-5/fillers/GFRP samples

Fig. 9 The relationship between the activation energy and conversion rate of **A** ZS/CNTs-GP, **B** ZS/GA-GP, **C** ZS/CB-GP samples

has a different E_a lead to appear these changes in the values of E_a [68, 69].

While the average E_a at each heating rate for all samples are shown in Fig. 10. In ZS/CNTs-GP sample, linear KAS (157 kJ mol^{-1}) and FWO (177 kJ mol^{-1}) models were applied, while Friedman model proved a high extreme value (230 kJ mol^{-1}) due to its aforementioned high sensitivity to noise data. The same features were

noticed in other samples (ZS/GA-GP and ZS/CB-GP) with some differences in E_a values, where ZS/CB-GP showed a higher value. Also, it was noticed that the average values of R2 for all conversion regions were located in the rages 0.823–0.874. The values are so low due to the fact that these kinds of models can be used to predict the reaction mechanism in the main conversion regions (20–80%). Therefore, having ignored lower and higher

Fig. 10 The calculated average activation energies of ZSM-5/fillers/GFRP samples
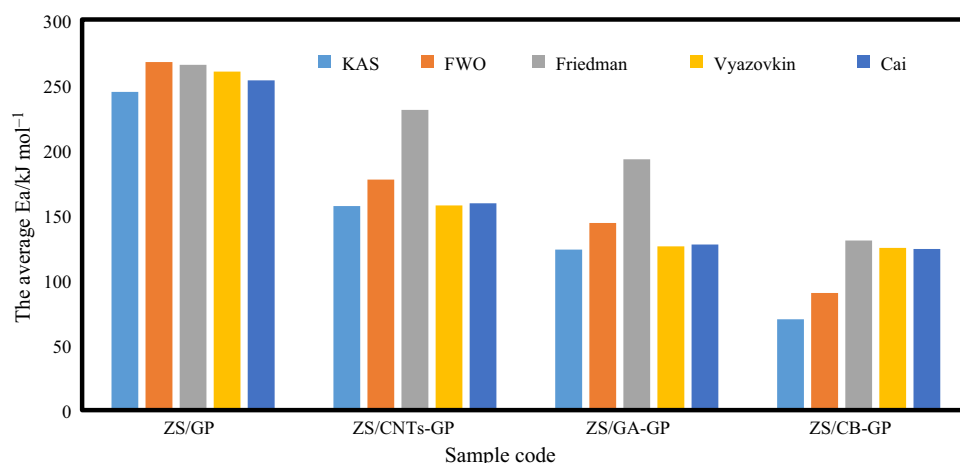
values, after recalculation of R^2, the values were estimated at > 0.85, being highly predictable values. When these E_a values were compared with the results of pyrolysis of GFRP (with and without catalyst) with E_a in the ranges 182.91–274.43 kJ mol^{-1} [19, 22, 23, 25], the present values were much easier.

Nonlinear isoconversional methods E_A for each conversion zone was determined numerically again using Vyazovkin and Cai nonlinear isoconversional methods (Eqs. (7, 8)) in order to get the right values of E_a in ranges of 10–90%. The optimal values of E_a were obtained after several iterations and the initial conditions used to run the built code of E_a were 200 kJ mol^{-1}. The E_a obtained at each conversion and iteration for all samples are listed in Table (S6, S7). It is clear the

average E_a obtained from both nonlinear models are almost similar (159 kJ mol^{-1}) with less R2 in the main conversion ranges. This means that nonlinear isoconversional models have higher predicted to simulate pyrolysis kinetics of ZSM-5/fillers/GFRP samples compared with linear methods. Based on the conditions used to calculate the optimal values, Vyazovkin and Cai curves were fitted as illustrated in Fig. 11 and the definition of Y-axes are provided in Eqs. (9, 10).

$$\ln\left\{\frac{\beta_i}{T_{y,i}^2\left[h(x_{y,i}) - \frac{x_{y,}^2\, e^{x_{\alpha,i}}}{x_{y,i-0.1}^2\, e^{x_{y,i-0.1}}}h(x_{y,i-0.1})\right]}\right\} \quad (12)$$
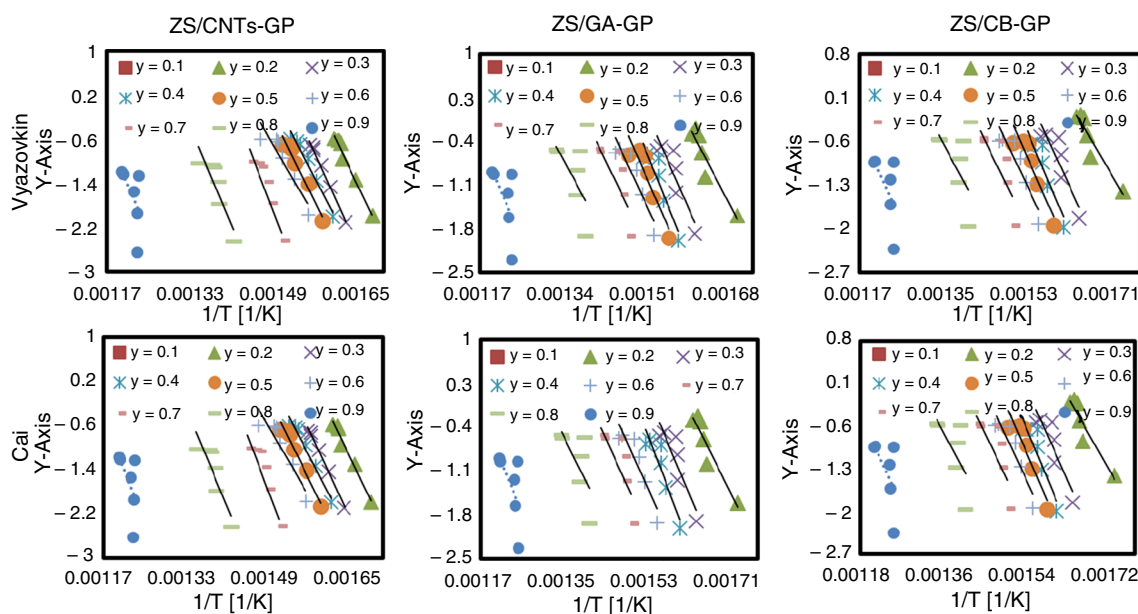
Fig. 11 Plots of nonlinear isoconversional relationships of ZSM-5/fillers/GFRP samples

Table 4 shows the kinetic parameters (E and A) calculated from DAEM and IPR models

Sample	ZS/CNTs-GP		ZS/GA-GP		ZS/CB-GP	
Model	DAEM	IPR	DAEM	IPR	DAEM	IPR
E1	176.65	161.41	145.7	134.12	90.05	82.28
A1	7.39E+16	2.92E+12	3.23E+12	1.35E+08	2.01E+09	7.93E+04
E2	219.05	206.87	183.9	172.32	111.667	105.46
A2	8.12E+16	3.11E+13	3.63E+12	1.43E+09	2.20E+09	8.43E+05

$$\ln\left\{\frac{\beta_i}{T_{\alpha,i}^2\left[h(x_{\alpha,i}) - \frac{x_{\alpha,i}^2 e^{x_{\alpha,i}}}{x_{\alpha-\Delta\alpha,i}^2 e^{x_\alpha \Delta\alpha,i}}h(x_{\alpha-\Delta\alpha,i})\right]}\right\} \qquad (13)$$

Prediction of TGA-DTG curves using DAEM and IPR models

The TGA and DTG experimental curves of ZSM-5/fillers/GFRP samples were predicted using DAEM and IPR models. Only fitting TGA and DTG curves at minimum and maximum heating rates (5 and 30 °C min^{-1}) are presented just to save time and space. In the presented figures, the TGA and DTG experimental curves were presented in black and blue solid lines, respectively, while the calculated data were presented in yellow and blue dotted lines. It is clear that DAEM model succeeded to predict the TGA profiles of ZSM-5/fillers/GFRP batches with a significant reduction in deviation values in the ranges 0.6–2 (depending on the composition of feedstock and heating rates). Similarly, IPR model shows high performance to predict DTG data with deviation values less than 2. Finally, the optimum values of activation energies (E1 and E2) and pre-exponential factors (A1 and A2) used in the fitting of TGA and DTG profiles are shown in Table 4 for optional upscaling.

Conclusions

In this work, the effect of adding fillers and catalyst on the pyrolysis GFRP and its kinetics and composition of the generated vapour products was studied. The pyrolysis experiments were conducted on GFRP reinforced by carbon nanotubes (CNTs), graphene (GA), and carbon black particles (CB) over ZSM catalyst. The chemical structure and the composition of vapour products were observed using thermogravimetric analysis coupled with FTIR and GC/MS. We modelled the catalytic pyrolysis behaviour and complexity using various linear and nonlinear models. The major discovered results are summarized as follows:

1. Aromatic benzene, O–H stretching, and phenol were the main functional groups and GC compounds; their presence was abundant, especially in case of CNTs (54%) and GA (57%).
2. The involvement of fillers and catalyst can decrease the pyrolytic activation energies of GFRP from the ranges of 182.91–274.43 kJ mol^{-1} to 124–158 kJ mol^{-1} based on kinetic studies using linear and nonlinear models. This confirms that the catalytic pyrolysis process of GFRP over nanofillers and a catalyst is very beneficial and continues to decrease the consumption of pyrolysis activation energy.
3. Also, the kinetic prediction results for simulation of TGA and DTG curves using DAEM and IPR showed a lighter performance for that purpose and smaller deviation (< 2).

Based on the experimental and kinetic modelling results, future studies of the effect of addition of fillers and catalyst to the pyrolysis of GFRP should be performed by bench-scale reactor to simulate the industrial scale and to calculate the yield and economic and environmental performance of the suggested treatment.

Declarations

Conflict of interest The authors declare that they have no known competing financial interests or personal relationships that could have appeared to influence the work reported in this paper.

References

1. Naqvi SR, Prabhakara HM, Bramer EA, Dierkes W, Akkerman R, Brem G. A critical review on recycling of end-of-life carbon fibre/glass fibre reinforced composites waste using pyrolysis towards a circular economy. Resour Conserv Recycl. 2018. https://doi.org/10.1016/j.resconrec.2018.04.013.

2. Tatariants M, Yousef S, Sidaraviciute R, Denafas G, Bendikiene R. Characterization of waste printed circuit boards recycled using a dissolution approach and ultrasonic treatment at low temperatures. RSC Adv. 2017. https://doi.org/10.1039/c7ra07034a.

3. Kimm M, Pico D, Gries T. Investigation of surface modification and volume content of glass and carbon fibres from fibre reinforced polymer waste for reinforcing concrete. J Hazard Mater. 2020. https://doi.org/10.1016/j.jhazmat.2019.121797.

4. Hao S, Kuah ATH, Rudd CD, Wong KH, Lai NYG, Mao J, et al. A circular economy approach to green energy: wind turbine, waste, and material recovery. Sci Total Environ. 2020. https://doi.org/10.1016/j.scitotenv.2019.135054.

5. Subadra SP, Yousef S, Griskevicius P, Makarevicius V. High-performance fiberglass/epoxy reinforced by functionalized CNTs for vehicle applications with less fuel consumption and greenhouse gas emissions. Polym Test. 2020. https://doi.org/10.1016/j.polymertesting.2020.106480.

6. Subadra SP, Griskevicius P, Yousef S. Low velocity impact and pseudo-ductile behaviour of carbon/glass/epoxy and carbon/glass/PMMA hybrid composite laminates for aircraft application at service temperature. Polym Test. 2020. https://doi.org/10.1016/j.polymertesting.2020.106711.

7. Cousins DS, Suzuki Y, Murray RE, Samaniuk JR, Stebner AP. Recycling glass fiber thermoplastic composites from wind turbine blades. J Clean Prod. 2019. https://doi.org/10.1016/j.jclepro.2018.10.286.

8. Jarek B, Kubik A. The examination of the glass fiber reinforced polymer composite rods in terms of the application for concrete reinforcement. Procedia Eng. 2015. https://doi.org/10.1016/j.proeng.2015.06.163.

9. Karuppannan Gopalraj S, Kärki T. A review on the recycling of waste carbon fibre/glass fibre-reinforced composites: fibre recovery, properties and life-cycle analysis. SN Appl Sci. 2020. https://doi.org/10.1007/s42452-020-2195-4.

10. Oliveux G, Dandy LO, Leeke GA. Current status of recycling of fibre reinforced polymers: review of technologies, reuse and resulting properties. Prog Mater Sci. 2015. https://doi.org/10.1016/j.pmatsci.2015.01.004.

11. Tatariants M, Denafas G, Bendikiene R. Separation and purification of metal and fiberglass extracted from waste printed circuit boards using milling and dissolution techniques. Environ Prog Sustain Energy. 2018. https://doi.org/10.1002/ep.12899.

12. Howarth J, Mareddy SSR, Mativenga PT. Energy intensity and environmental analysis of mechanical recycling of carbon fibre composite. J Clean Prod. 2014. https://doi.org/10.1016/j.jclepro.2014.06.023.

13. Onwudili JA, Miskolczi N, Nagy T, Lipóczi G. Recovery of glass fibre and carbon fibres from reinforced thermosets by batch pyrolysis and investigation of fibre re-using as reinforcement in LDPE matrix. Compos Part B Eng. 2016. https://doi.org/10.1016/j.compositesb.2016.01.055.

14. Tatariants M, Bendikiene R, Kriūkienė R, Denafas G. A new industrial technology for closing the loop of full-size waste motherboards using chemical-ultrasonic-mechanical treatment. Proc Saf Environ Prot. 2020. https://doi.org/10.1016/j.psep.2020.04.002.

15. Tatariants M, Tichonovas M, Bendikiene R, Denafas G. Recycling of bare waste printed circuit boards as received using an organic solvent technique at a low temperature. J Clean Prod. 2018. https://doi.org/10.1016/j.jclepro.2018.03.227.

16. Tatariants M, Bendikiene R, Denafas G. Mechanical and thermal characterizations of non-metallic components recycled from waste printed circuit boards. J Clean Prod. 2017. https://doi.org/10.1016/j.jclepro.2017.08.195.

17. Yun YM, Seo MW, Ra HW, Koo GH, Oh JS, Yoon SJ, et al. Pyrolysis characteristics of glass fiber-reinforced plastic (GFRP) under isothermal conditions. J Anal Appl Pyrolysis. 2015. https://doi.org/10.1016/j.jaap.2015.04.013.

18. Yun YM, Seo MW, Koo GH, Ra HW, Yoon SJ, Kim YK, et al. Pyrolysis characteristics of GFRP (glass fiber reinforced plastic) under non-isothermal conditions. Fuel. 2014. https://doi.org/10.1016/j.fuel.2014.08.001.

19. Eimontas J, Striūgas N, Praspaliauskas M, Abdelnaby MA. Pyrolysis kinetic behaviour of glass fibre-reinforced epoxy resin composites using linear and nonlinear isoconversional methods. Polymers. 2021. https://doi.org/10.3390/polym13101543.

20. Qiao Y, Das O, Zhao SN, Sun TS, Xu Q, Jiang L. Pyrolysis kinetic study and reaction mechanism of epoxy glass fiber reinforced plastic by thermogravimetric analyzer (Tg) and tg–ftir (fourier-transform infrared) techniques. Polymers. 2020. https://doi.org/10.3390/polym12112739.

21. Ma C, Sánchez-Rodríguez D, Kamo T. A comprehensive study on the oxidative pyrolysis of epoxy resin from fiber/epoxy composites: product characteristics and kinetics. J Hazard Mater. 2021. https://doi.org/10.1016/j.jhazmat.2021.125329.

22. Eimontas J, Striūgas N, Abdelnaby MA. Influence of carbon black filler on pyrolysis kinetic behaviour and TG-FTIR-GC–MS analysis of glass fibre reinforced polymer composites. Energy. 2021. https://doi.org/10.1016/j.energy.2021.121167.

23. Yousef S, Eimontas J, Striūgas N, Abdelnaby MA. Thermal decomposition of CNTs and graphene-reinforced glass fibers/epoxy and their kinetics. Biomass Convers Biorefinery. 2022. https://doi.org/10.1007/s13399-022-02341-3.

24. Kim YM, Han TU, Kim S, Jae J, Jeon JK, Jung SC, et al. Catalytic co-pyrolysis of epoxy-printed circuit board and plastics over HZSM-5 and HY. J Clean Prod. 2017. https://doi.org/10.1016/j.jclepro.2017.08.224.

25. Kiminaitė I, Eimontas J, Striūgas N, Abdelnaby MA. Catalytic pyrolysis kinetic behaviour of glass fibre-reinforced epoxy resin composites over ZSM-5 zeolite catalyst. Fuel. 2022. https://doi.org/10.1016/j.fuel.2022.123235.

26. Mohamed A. Mass production of CNTs using CVD multi-quartz tubes. J Mech Sci Technol. 2016. https://doi.org/10.1007/s12206-016-1031-7.

27. Mohamed A, Tatariants M. Mass production of graphene nanosheets by multi-roll milling technique. Tribol Int. 2018. https://doi.org/10.1016/j.triboint.2018.01.040.

28. Subadra SP, Griškevičius P, Varnagiris S, Milcius D, Makarevicius V. Superhydrophilic functionalized graphene/fiberglass/epoxy laminates with high mechanical, impact and thermal performance and treated by plasma. Polym Test. 2020. https://doi.org/10.1016/j.polymertesting.2020.106701.

29. Eimontas J, Subadra SP, Striūgas N. Functionalization of char derived from pyrolysis of metallised food packaging plastics waste and its application as a filler in fiberglass/epoxy composites. Proc Saf Environ Prot. 2021. https://doi.org/10.1016/j.psep.2021.01.009.

30. Abdelnaby MA, Eimontas J, Striūgas N. Catalytic pyrolysis kinetic behavior and TG-FTIR-GC–MS analysis of metallized food packaging plastics with different concentrations of ZSM-5 zeolite catalyst. Polymers. 2021. https://doi.org/10.3390/polym13050702.

31. https://www.acsmaterial.com/zsm-5-catalyst.html

32. Eimontas J, Striūgas N, Abdelnaby MA. Pyrolysis and gasification kinetic behavior of mango seed shells using TG-FTIR-GC–MS system under N2 and CO2 atmospheres. Renew Energy. 2021. https://doi.org/10.1016/j.renene.2021.04.034.

33. Striūgas N, Eimontas J, Subadra SP, Abdelnaby MA. Thermal degradation and pyrolysis kinetic behaviour of glass fibre-reinforced thermoplastic resin by TG-FTIR, Py-GC/MS, linear and nonlinear isoconversional models. J Mater Res Technol. 2021. https://doi.org/10.1016/j.jmrt.2021.11.011.

34. Eimontas J, Striūgas N, Abdelnaby MA. Pyrolysis kinetic behaviour and TG-FTIR-GC–MS analysis of coronavirus face masks. J Anal Appl Pyrolysis. 2021. https://doi.org/10.1016/j.jaap.2021.105118.

35. Mohamed A, Eimontas J, Striūgas N, Abdelnaby MA. Morphology, compositions, thermal behavior and kinetics of pyrolysis of lint-microfibers generated from clothes dryer. J Anal Appl Pyrolysis. 2021. https://doi.org/10.1016/j.jaap.2021.105037.

36. Ali Abdelnaby M, Eimontas J, Striūgas N, Mohamed A. Pyrolysis kinetic behavior and TG-FTIR-GC–MS analysis of end-life ultrafiltration polymer nanocomposite membranes. Chem Eng J. 2022. https://doi.org/10.1016/j.cej.2021.131181.

37. Praspaliauskas M, Eimontas J, Striūgas N, Zakarauskas K, Abdelnaby MA. Pyrolysis kinetic behavior and TG-FTIR-GC–MS analysis of metallised food packaging plastics. Fuel. 2020. https://doi.org/10.1016/j.fuel.2020.118737.

38. Abdelnaby MA, Eimontas J, Striugas N. Modeling of metalized food packaging plastics pyrolysis kinetics using an independent parallel reactions kinetic model. Polymers. 2020. https://doi.org/10.3390/polym12081763.

39. Eimontas J, Striūgas N, Abdelnaby MA. Catalytic pyrolysis kinetic behaviour and TG-FTIR-GC–MS analysis of waste fishing nets over ZSM-5 zeolite catalyst for caprolactam recovery. Renew Energy. 2021. https://doi.org/10.1016/j.renene.2021.07.143.

40. Fredi G, Dorigato A, Fambri L, Pegoretti A. Multifunctional epoxy/carbon fiber laminates for thermal energy storage and release. Compos Sci Technol. 2018. https://doi.org/10.1016/j.compscitech.2018.02.005.

41. Tatariants M, Sidaraviciute R, Denafas G, Bendikiene R. Characterization of waste printed circuit boards recycled using a dissolution approach and ultrasonic treatment at low temperatures. RSC Adv. 2017. https://doi.org/10.1039/C7RA07034A.

42. Wang B, Xu F, Zong P, Zhang J, Tian Y, Qiao Y. Effects of heating rate on fast pyrolysis behavior and product distribution of Jerusalem artichoke stalk by using TG-FTIR and Py-GC/MS. Renew Energy. 2019. https://doi.org/10.1016/j.renene.2018.08.021.

43. Ma M, Bai Y, Wang J, Lv P, Song X, Su W, et al. Study on the pyrolysis characteristics and kinetic mechanism of cow manure under different leaching solvents pretreatment. J Environ Manag. 2021. https://doi.org/10.1016/j.jenvman.2021.112580.

44. Hu H, Shu R, Meng L, Yu T, Wang C, Chen D, et al. Tribological and thermal characteristics of an epoxy-based composite containing polyaryletherketone. High Perform Polym. 2022. https://doi.org/10.1177/09540083211069039.

45. Kremer I, Tomić T, Katančić Z, Erceg M, Papuga S, Parlov Vuković J, et al. Catalytic pyrolysis and kinetic study of real-world waste plastics: multi-layered and mixed resin types of plastics. Clean Technol Environ Policy. 2022. https://doi.org/10.1007/s10098-021-02196-8.

46. Cui L, Zhang Y, Du X, Wei G. Computational study on thermal conductivity of defective carbon nanomaterials: carbon nanotubes versus graphene nanoribbons. J Mater Sci. 2018. https://doi.org/10.1007/s10853-017-1874-z.

47. Seyed M, Sara E, Hediyeh K, Mohammad M, Nouranian S, Seyed J, et al. A review of electrical and thermal conductivities of epoxy resin systems reinforced with carbon nanotubes and graphene-based nanoparticles. Polym Test. 2022. https://doi.org/10.1016/j.polymertesting.2022.107645.

48. Li Y, Nishu YD, Chai M, Li C, Liu R. Catalytic pyrolysis of biomass over Fe-modified hierarchical ZSM-5: insights into mono-aromatics selectivity and pyrolysis behavior using Py-GC/MS and TG-FTIR. J Energy Inst. 2021. https://doi.org/10.1016/j.joei.2021.09.013.

49. Aragaw TA, Mekonnen BA. Current plastics pollution threats due to COVID-19 and its possible mitigation techniques: a waste-to-energy conversion via Pyrolysis. Environ Syst Res. 2021. https://doi.org/10.1186/s40068-020-00217-x.

50. Feng T, Wang Y, Dong H, Piao J, Wang Y, Ren J, et al. Ionic liquid modified boron nitride nanosheets for interface engineering of epoxy resin nanocomposites: improving thermal stability, flame retardancy, and smoke suppression. Polym Degrad Stab. 2022. https://doi.org/10.1016/j.polymdegradstab.2022.109899.

51. Chen Y, Duan H, Ji S, Ma H. Novel phosphorus/nitrogen/boron-containing carboxylic acid as co-curing agent for fire safety of epoxy resin with enhanced mechanical properties. J Hazard Mater. 2021. https://doi.org/10.1016/j.jhazmat.2020.123769.

52. Eimontas J, Zakarauskas K, Striūgas N. Microcrystalline paraffin wax, biogas, carbon particles and aluminum recovery from metallised food packaging plastics using pyrolysis, mechanical and chemical treatments. J Clean Prod. 2021. https://doi.org/10.1016/j.jclepro.2021.125878.

53. Zakarauskas K, Eimontas J, Striūgas N, Mohamed A. A new strategy for using lint-microfibers generated from clothes dryer as a sustainable source of renewable energy. Sci Total Environ. 2021. https://doi.org/10.1016/j.scitotenv.2020.143107.

54. Kuliešienė N, Sakalauskaitė S, Nenartavičius T, Daugelavičius R. Sustainable green strategy for recovery of glucose from end-of-life euro banknotes. Waste Manag. 2021. https://doi.org/10.1016/j.wasman.2021.01.007.

55. Long TR, Knorr DB, Masser KA, Elder RM, Sirk TW, Hindenlang MD, et al. Ballistic response of polydicyclopentadiene vs epoxy resins and effects of crosslinking. Conf Proc Soc Exp Mech Ser. 2017. https://doi.org/10.1007/978-3-319-41132-3_37.

56. Pender K, Yang L. Investigation of the potential for catalysed thermal recycling in glass fibre reinforced polymer composites by using metal oxides. Compos Part A Appl Sci Manuf. 2017. https://doi.org/10.1016/j.compositesa.2017.05.016.

57. Datsyuk V, Trotsenko S, Trakakis G, Boden A, Vyzas-Asimakopoulos K, Parthenios J, et al. Thermal properties enhancement of epoxy resins by incorporating polybenzimidazole nanofibers filled with graphene and carbon nanotubes as reinforcing material. Polym Test. 2020. https://doi.org/10.1016/j.polymertesting.2019.106317.

58. Serrano DP, Melero JA, Morales G, Iglesias J, Pizarro P. Progress in the design of zeolite catalysts for biomass conversion into biofuels and bio-based chemicals. Catal Rev Sci Eng. 2018. https://doi.org/10.1080/01614940.2017.1389109.

59. Ali S, Abdelnaby MA, Christova D, Hassan Y, Samir D, et al. Synthesis and characterization of CNTs/POM nanocomposite acetabular hip cup. Int J Polym Mater Polym Biomater. 2018. https://doi.org/10.1080/00914037.2017.1362641.

60. Visco A, Galtieri G, Nocita D, Pistone A, Njuguna J. Thermal, mechanical and rheological behaviors of nanocomposites based on UHMWPE/paraffin oil/carbon nanofiller obtained by using different dispersion techniques. JOM. 2016. https://doi.org/10.1007/s11837-016-1845-x.

61. Sarwar Z, Tatariants M, Krugly E, Čiužas D, Danilovas PP, et al. Fibrous PEBA-graphene nanocomposite filaments and membranes fabricated by extrusion and additive manufacturing. Eur Polym J. 2019. https://doi.org/10.1016/j.eurpolymj.2019.109317.

62. Mohamed A, Nasser WS, Osman TA, Knebel A, Sánchez EPV, et al. Rapid photocatalytic degradation of phenol from water using

composite nanofibers under UV. Environ Sci Eur. 2020. https://doi.org/10.1186/s12302-020-00436-0.

63. Thallada B, Kumar A, Jindal M, Maharana S. Lignin biorefinery: new horizons in catalytic hydrodeoxygenation for the production of chemicals. Energy Fuels. 2021. https://doi.org/10.1021/acs.energyfuels.1c01651.

64. Kalpokaitė-Dičkuvienė R, Baltušnikas A, Pitak I, Lukošiūtė SI. A new strategy for functionalization of char derived from pyrolysis of textile waste and its application as hybrid fillers (CNTs/char and graphene/char) in cement industry. J Clean Prod. 2021. https://doi.org/10.1016/j.jclepro.2021.128058.

65. Eimontas J, Striūgas N, Abdelnaby MA. Gasification kinetics of char derived from metallised food packaging plastics waste pyrolysis. Energy. 2022. https://doi.org/10.1016/j.energy.2021.122070.

66. Schulz H. From the Kissinger equation to model-free kinetics: reaction kinetics of thermally initiated solid-state reactions. ChemTexts. 2018. https://doi.org/10.1007/s40828-018-0062-3.

67. Torres-Herrador F, Eschenbacher A, Blondeau J, Magin TE, Van Geem KM. Study of the degradation of epoxy resins used in spacecraft components by thermogravimetry and fast pyrolysis. J Anal Appl Pyrolysis. 2022. https://doi.org/10.1016/j.jaap.2021.105397.

68. Meng A, Chen S, Long Y, Zhou H, Zhang Y, Li Q. Pyrolysis and gasification of typical components in wastes with macro-TGA. Waste Manag. 2015. https://doi.org/10.1016/j.wasman.2015.08.025.

69. Pinzi S, Buratti C, Bartocci P, Marseglia G, Fantozzi F, Barbanera M. A simplified method for kinetic modeling of coffee silver skin pyrolysis by coupling pseudo-components peaks deconvolution analysis and model free-isoconversional methods. Fuel. 2020. https://doi.org/10.1016/j.fuel.2020.118260.